Influence of synthesis experimental parameters on the formation of magnetite nanoparticles prepared by polyol method

# Influence of synthesis experimental parameters on the formation of magnetite nanoparticles prepared by polyol method

**Jaime Vega-Chacón[1,2], Gino Picasso[2], Luis Avilés-Félix[3,4] and Miguel Jafelicci Jr[1]**

[1] Laboratory of Magnetic Materials and Colloids, Institute of Chemistry, São Paulo State University (UNESP), Araraquara, São Paolo, Brazil
[2] Laboratory of Physical Chemistry Research, Faculty of Sciences, National University of Engineering, Av. Túpac Amaru 210, Rimac, Lima, Peru
[3] Consejo Nacional de Investigaciones Científicas y Técnicas, Centro Atómico Bariloche, CNEA, Bustillo 9500, 8400 Bariloche, Argentina
[4] Instituto Balseiro, Universidad Nacional de Cuyo & CNEA, 8400 Bariloche, Argentina

E-mail: jvegachacon@gmail.com

CrossMark

## Abstract

In this paper we present a modified polyol method for synthesizing magnetite nanoparticles using iron (III) nitrate, a low toxic and cheap precursor salt. The influence of the precursor salt nature and initial ferric concentration in the average particle size and magnetic properties of the obtained nanoparticles were investigated. Magnetite nanoparticles have received much attention due to the multiple uses in the biomedical field; for these purposes nanoparticles with monodisperse size distribution, superparamagnetic behavior and a combination between small average size and high saturation magnetization are required. The polyol conventional method allows synthesizing water-dispersible magnetite nanoparticles with these features employing iron (III) acetylacetonate as precursor salt. Although the particle sizes of samples synthesized from the conventional polyol method (denoted CM) are larger than those of samples synthesized from the modified method (denoted MM), they display similar saturation magnetization. The differences in the nanoparticles average sizes of samples CM and samples MM were explained though the known nanoparticle formation mechanism.

Keywords: superparamagnetic magnetite, thermal decomposition, polyol method, magnetite nanoparticle
Classification numbers: 2.03, 4.02, 5.02

## 1. Introduction

Magnetite nanoparticles are one of the few magnetic responsive materials with low toxicity in humans, with the ability to function at the cellular and molecular level of biological interactions. These particles can also exhibit super-paramagnetism, a magnetic behavior in which the nanoparticles are only magnetized in the presence of an external magnetic field, avoiding the agglomeration process of the nanoparticles. All these characteristics have attracted increasing interest in the last years for the use of magnetite nanoparticles in biomedical applications including: magnetically controlled transport of drugs, genes and proteins, contrast agents in biomedical imaging, target to be used in the restore of tissues, magnetic hyperthermia treatment, bioanalysis among others [1–8]. Magnetite nanoparticles have been prepared by different methods such as coprecipitation [9], sonochemistry [10], hydrothermal method [11], reversed

microemulsion [12] and thermal decomposition of metal organometallic compounds [13]. All these methods allowed obtaining stable nanocrystals of magnetite, although the elementary steps of each method involve different mechanisms and require to a greater or lesser extent different thermal treatments and starting material consumption in addition to energy use and time for their synthesis and application at large scale.

Among various preparation methods of synthesis of magnetite, thermal decomposition in organic phase solution of an iron precursor is considered one of the most interesting approaches due to production of monodisperse nanocrystals. The size and shape of the nanocrystals could be also controlled by variation of the concentration and reactivity of the precursors, solvents and surfactants [14]. This method presents, in turn, different variants. One of them, introduced by Rockenberger *et al* [15], is the decomposition of iron precursor in a high boiling point solvent with the assistance of surfactants such as oleic acid and oleylamine, among others [16]. However, magnetic nanoparticles are suspended in nonpolar solvents due to the hydrophobic nature of surfactants that restrict biomedical applications [17]. The second option is based on the polyol method, which is a suitable variant of thermal decomposition synthesis dealing to monodisperse metal and metal oxide nanoparticles [18, 19]. The synthesis of magnetite nanoparticle by polyol method was introduced by Cai and Wan [20], which consists of the decomposition of iron (III) acetylacetonate in a polyol as solvent, finding that triethylene glycol (TEG) is the best solvent which allows us to obtain, in only one step, monodispersed hydrophilic magnetite nanoparticles. This procedure represents an important step for the utilization of monodisperse magnetite nanoparticles in biomedicine applications. Other works studying the characteristics of the obtained nanoparticles were reported after the work of Cai and Wan [21–26]. Miguel-Sancho *et al* [24] discussed the stability of nanoparticles in relation with agglomeration process by using either dimercaptosuccinicacid (DMSA) or chemical modification of TEG coating. In a more recent paper, Miguel-Sancho *et al* [25] showed the influence of some experimental parameters on particle size, as initial precursor concentration, decomposition time and heating rate. A particle formation mechanism of iron oxide nanoparticles was proposed, which could be controlled by the total Fe(acac)$_3$ concentration and the type of solvent used, although crystallization conditions and magnetic properties were not discussed. Grabs *et al* [21] compared decomposition of Fe(acac)$_3$ in TEG and benzyl alcohol and evaluated how the reaction time affects the crystalline and magnetic properties, maintaining a constant concentration of the precursor. Jiang *et al* [27] modified the method using ferric nitrate as precursor salt, obtaining very small iron oxide nanoparticle, however the influence of the initial concentration of the precursor salt and a comparative study with the conventional method were not reported. Arndt *et al* [28] extended the method introducing structure-directing agents and studied the influence of the experimental parameters on the characteristics of the produced nanoparticles.

In previous work some general properties of magnetite nanoparticles regarding textural, structural and magnetic features and their relation with preparation conditions were studied [29]. However, the particle size distribution was polydisperse and there was no relation with magnetic properties. In this paper, magnetite nanoparticles were synthesized by decomposition in organic media with the polyol approach in order to obtain uniform and highly crystalline and colloidaly stable superparamagnetic nanoparticles, using iron (III) acetylacetonate and iron (III) nitrate as precursors with different initial concentration leading to achieve monodisperse superparamagnetic Fe$_3$O$_4$ nanoparticles. The influence of both the nature and the initial ferric concentration of precursor salt on the degree of crystallinity, average particle size and magnetic properties have been investigated.

## 2. Experimental

### 2.1. Preparation of magnetite nanoparticles

All the reagents were analytical grade and used as purchased. The starting material, ethyl acetate, triethylene glycol (TEG, 99%) and iron (III) nitrate nonahydrate (Fe(NO$_3$)$_3$.9H$_2$O, 99%) were purchased from Merck, meanwhile iron (III) acetylacetonate (Fe(acac)$_3$, 97%) and ethanol obtained from Sigma-Aldrich.

Water-dispersible magnetite nanoparticles were prepared by the thermal decomposition of Fe(acac)$_3$ or Fe(NO$_3$)$_3$.9H$_2$O in TEG at 280 °C according to Cai and Wan [20].

The magnetite nanoparticles prepared from iron (III) acetylacetonate and iron (III) nitrate were nominated as samples CM and samples MM, respectively. Samples of different initial Fe$^{3+}$ concentration (IC) of 0.06 mol L$^{-1}$ (CM1 and MM1); 0.10 mol L$^{-1}$ (CM2 and MM2) and 0.15 mol L$^{-1}$ (CM3 and MM3) were prepared.

A certain amount of ferric salt was dissolved in 80 ml of TEG in a three-necked round-bottomed flask equipped with a condenser, heated at 120 °C for 30 min with magnetic stirring and then, solution temperature was increased up to 180 °C and maintained for 30 min. Thereby, the temperature of the solution was increased up to 280 °C for 60 min, afterwards the suspension was cooled to room temperature. A mixture of 60 ml of ethyl acetate and 10 ml of ethanol was added to the resulting colloidal dispersion in order to allow nanoparticles flocculation. The nanoparticles were separated from the dispersion medium by a magnetic-field-assisted sedimentation procedure with a neodymium magnet and this operation was repeated until the supernatant rested colorless. The nanoparticles were dispersed in deionized water and a fraction of the nanoparticles were dried in a vacuum oven at 50 °C.

### 2.2. Characterization of magnetite samples

XRD analysis was performed on a RIGAKU Miniflex model operating with the following parameters: Cu K$\alpha$ radiation ($\lambda = 1.5418$ Å), 15 mA, 30 kV, Ni filter, $2\theta$ scanning range 20–70° with a step size of 0.10° and a step time of 2.5 s. The
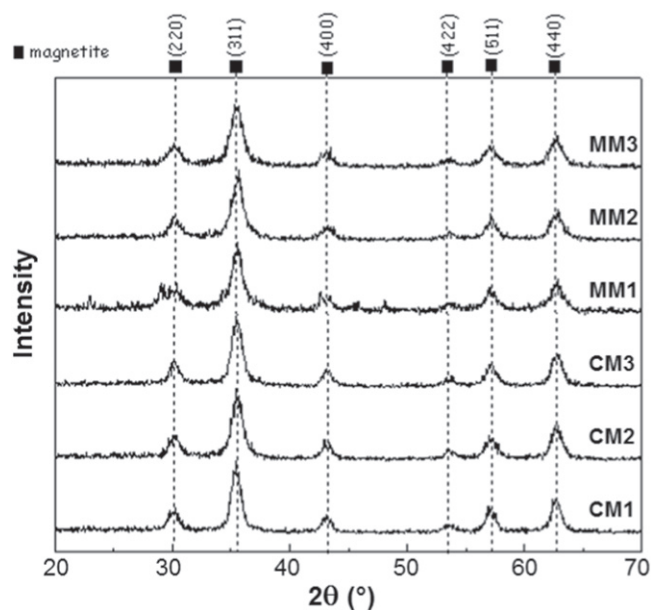
**Figure 1.** XRD patterns of magnetite samples from iron (III) acetylacetonate and iron (III) nitrate precursors, respectively, CM and MM.



**Figure 2.** FTIR spectra of samples MM1and CM1.

crystal phases were identified using diffraction data from JCPDS (International Centre for Diffraction Data).

FTIR spectra of dried samples diluted in KBr were recorded in transmission mode by spectrophotometer FTIR, Nicolet Model 410 Impact 410.

Size and morphology of the nanoparticles were determined by transmission electron microscope (TEM, Philips CM-120) at 120 kV. Dilute alcohol suspension of every specimen was dropped onto a carbon-coated copper grind and dried prior to analysis. It was measured the size of at least 100 nanoparticles using the software ImageJ, the average diameter and the standard deviation were calculated assuming a log-normal distribution.

Magnetic properties of magnetite nanoparticles were measured with a LakeShore VSM magnetometer with 10 kOe maximum field. Magnetization of the nanoparticles was measured at 85 K and 300 K. The saturation magnetization ($M_s$) was obtained according to Roca *et al* [30].

## 3. Results and discussion

XRD diffractograms are shown in figure 1, peaks matched in position and in relative intensity to the characteristic pattern corresponding to inverse spinel of magnetite $Fe_3O_4$ (JCPDS —International Centre for Diffraction Data N° 33-0664). The black color of the powders confirms that magnetite is the mainly phase in the samples [31]. The sample MM1 presents a broader peak at 30° which could be attributed to the distortion arrangement of surface atoms in relation to inner atoms of the particle. The fractions of atoms presented on the surface of a particle increase when the particle size decrease, expanding also the distortions within the particle [14, 32].
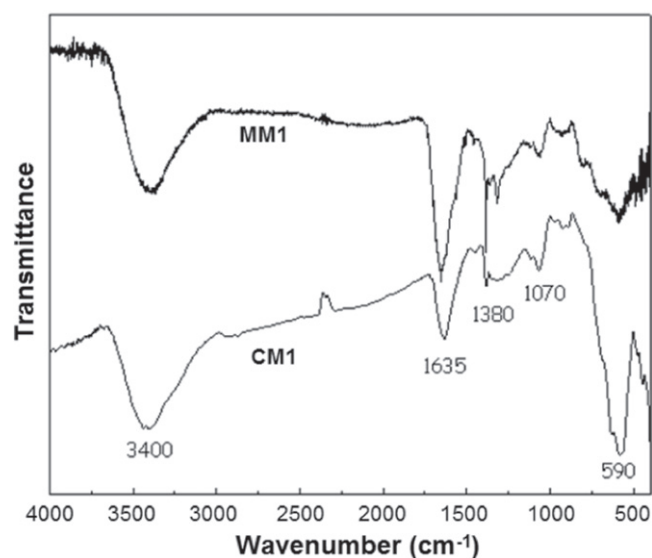
As will be seen later, the sample MM1 had the lowest average particle size, therefore such distortions were expected.

FTIR spectra of samples CM1 and MM1 are shown in figure 2. The broad band centered at 3400 cm$^{-1}$ is assigned to hydrogen bonded O–H stretching vibration of water and TEG adsorbed to the nanoparticles surface. The band at 1635 cm$^{-1}$ is due to the H-O-H bending mode of the remaining water in the sample [26]. The band observed at 1070 cm$^{-1}$ is due to C-O stretching vibration which confirms the presence of TEG over the particle surface [20]. Both samples exhibit a band centered at about 590 cm$^{-1}$, assigned to the Fe–O stretching vibration for the magnetite nanoparticles [20], however, in the case of CM1 this band is stronger and narrower than the corresponding to MM1. The main difference between both samples is the extra band in MM1, at about 1380 cm$^{-1}$, possibly related to the remaining nitrate species on the particle surface [33]. FTIR analysis confirmed that the samples consist of magnetite particles with organic hydrophilic molecules as TEG attached to the surface of the particles, which were responsible for the water-dispersibility of the nano-particles [34].

TEM images showed in figure 3 confirm the presence of nanoparticles with monodisperse size distributions. The observed morphology of samples CM1, CM2 and CM3 was spherical with minimum aggregation of nanoparticles, meanwhile samples MM1, MM2 and MM3 presented lesser regularity in the particle shape near to spherical.

The measured average particle size of samples is shown in table 1. The higher concentration of metal precursor, independently from its nature, increases the size of the particle. This effect was reported in the literature on the synthesis of magnetite nanoparticles by thermal decomposition method [25, 35].

Comparing samples with the same IC and different pre-cursor, the particle size corresponding to samples CM has been always larger than their MM counterparts. These differences were probably due to the nature of the precursor
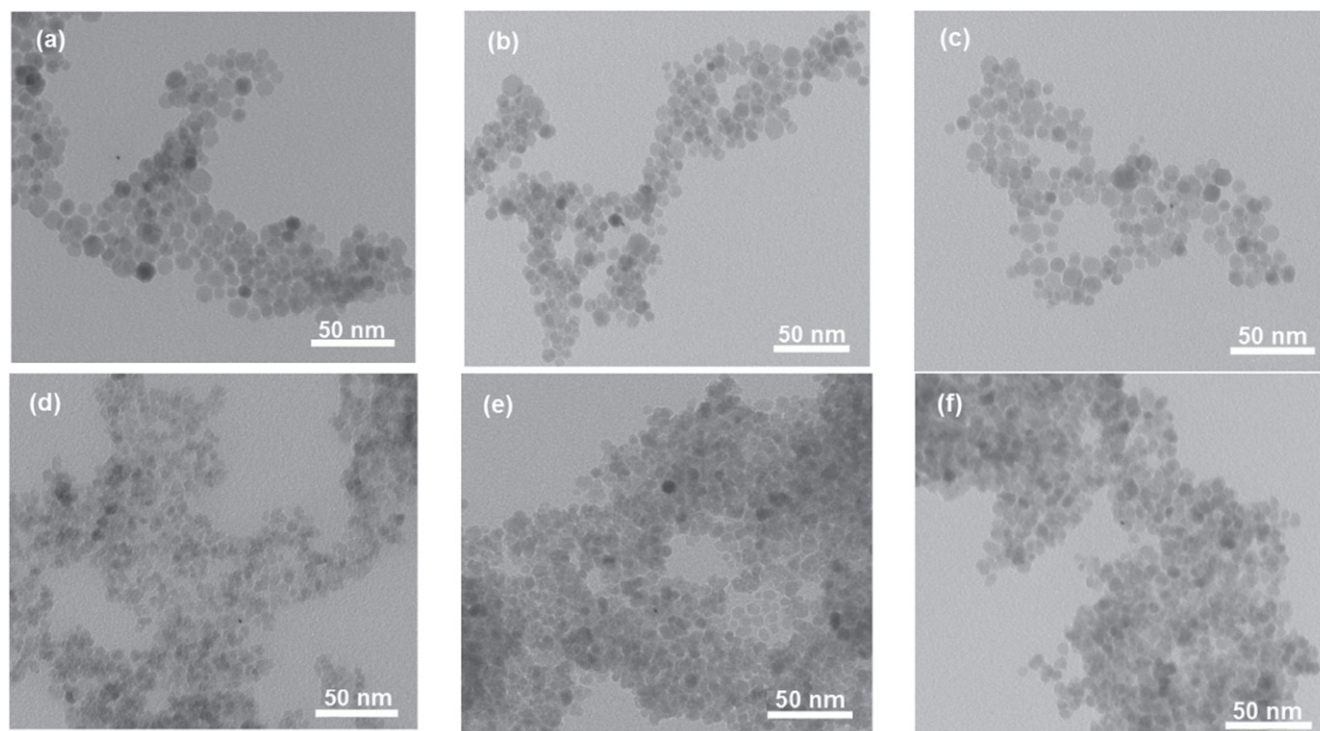
**Figure 3.** TEM micrographs of (a) CM1, (b) CM2, (c) CM3, (d) MM1, (e) MM2 and (f) MM3.

**Table 1.** Average particle size of nanoparticles evaluated by TEM and their corresponding magnetization and coercivity field values measured at 85 K and 300 K.

| Sample | IC (mol. $L^{-1}$) | $D_{TEM}$ (nm) | $M_s^{300K}$ (emu/g) | $M_s^{85K}$ (emu/g) | $H_c^{85K}$ (Oe) |
|--------|--------|--------|--------|--------|--------|
| CM1 | 0.06 | $9.0 \pm 1.3$ | 49.2 | 63.7 | 26 |
| CM2 | 0.10 | $9.2 \pm 1.6$ | 51.3 | 66.5 | 19 |
| CM3 | 0.15 | $9.6 \pm 1.8$ | 62.6 | 68.4 | 30 |
| MM1 | 0.06 | $4.4 \pm 0.7$ | 39.2 | 49.4 | 3 |
| MM2 | 0.10 | $6.0 \pm 0.7$ | 52.0 | 64.3 | 5 |
| MM3 | 0.15 | $6.1 \pm 0.8$ | 54.3 | 66.1 | 2 |

which sharply influenced the mechanism of nucleation and growth of particles in samples.

To interpret the microscopy results it is important to consider the mechanism of the magnetite nanoparticles formation. Such mechanism by thermal decomposition method can be understood following LaMer model of nucleation, which involves the formation of a metal complex by the dissolution of metal precursor in an organic solvent with high-boiling temperature and usually in the presence of surfactant molecules that act as ligands. The temperature of the mixture increases to the temperature at which the metal complex is unstable and starts to decompose into intermediate species that will act as monomers or building blocks of the nanoparticles. The concentration of intermediate species increases until reaching a high level of supersaturation at which a new phase, nuclei, is formed spontaneously consuming the intermediate species; this process is known as homogeneous nucleation. The nucleation reduces the concentration of the monomers until no more nucleation proceeds. The remained monomers precipitate on the surface of the nuclei, and the primary particles increase its dimensions continuously; this stage is known as growth process. Typically, the formed nanoparticles acquire uniform morphological characteristics since nucleation and the growth process are entirely separated steps in the time due to the fact that nucleation rate is adequately high [36, 37].

In the case of magnetite nanoparticles synthesized by the polyol method, the metal precursor is a ferric salt and TEG acts simultaneously as an organic hydrophilic solvent, a reducing agent, producing enough ions $Fe^{2+}$ for magnetite formation, and a stabilizer preventing the aggregation of nanoparticles [38]. As the temperature is increased, the solvolysis of the precursor takes place, but the exact nature of the formed iron complexes is still unknown. Some investigations suggest that TEG or a derivative compound of TEG is coordinated to the iron center [21, 25, 27]. When the temperature of the mixture is near to 180 °C, the color of the solution changes continuously from dark red to black, indicating the decomposition of the iron complexes and the nuclei formation in the solution. The further increasing of the temperature above 180 °C, enhances the monomer diffusion over the surface of the nanoparticles, increasing the growth rate, and also upgrading the crystallinity of the particles [24, 25].

A set of three consecutive reactions has been considered to explain the TEM results. In reaction 1, the solvolysis process of the precursors (FeL₃), where L is a nitrate group for samples MM and an acetylacetonate group for samples CM. In reaction 2, the decomposition of the iron complex formed in reaction 1 produces the intermediate species

Adv. Nat. Sci.: Nanosci. Nanotechnol. **7** (2016) 015014

J Vega-Chacón *et al*

represented as $FeA_x$. Reaction 3 shows the formation of the magnetite nanoparticles through the precipitation of the intermediate species.

$$FeL_3 + TEG \rightleftarrows FeL_2TEG + L, \tag{1}$$

$$FeL_2TEG \rightarrow FeA_x, \tag{2}$$

$$FeA_x \leftrightarrows Fe_3O_4. \tag{3}$$
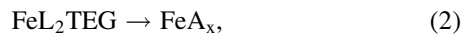
In samples MM, the vigorous liberation of a reddish-brown gas ($NO_X$) was observed, before reaching 180 °C, produced by the decomposition of the nitrate group [27]. The elimination of nitrate favors the formation of the iron complex (reaction 1), thereby, the precursor is completely transformed into the iron complex. According to Miguel-Sancho *et al* [25], there was no gas emission before 180 °C when the precursor was $Fe(acac)_3$, thus the formation of the iron complex, in samples CM, is limited by the equilibrium in reaction 1. From the previous discussion, at the same initial $Fe^{3+}$ concentration, the amount of iron complex in samples MM is higher than the corresponding one to samples CM, whatever the type of iron complex produced in reaction 1. Then, the amount of the intermediate species, obtained by the decomposition of the iron complex (reaction 2), and the extent of supersaturation (S) before the nucleation of samples MM is higher than the corresponding one to samples CM: $S_{MM} > S_{CM}$.

The classical theory of nucleation defines the critical radius ($r_c$) of nuclei, as the minimum radius of nuclei that can resist the dissolution and growth to form the nanoparticle [36]. The $r_c$ could be calculated from the following equation:

$$r_c = \frac{2\gamma V_m}{RT \ln S}, \tag{4}$$

where $\gamma$, is the surface free energy per unit area, $V_m$ is the molar volume of the monomer in crystal, $R$ is the universal gas constant and $T$ is the temperature.

Due to $S_{MM} > S_{CM}$, it was concluded that the critical radius of nuclei produced in samples MM is lower than in samples CM, at the same temperature: $r_c^{MM} < r_c^{CM}$.

Moreover, after the nucleation process in samples CM, more intermediate species were generated from the remained precursor that were not totally transformed into iron complex before the nucleation (reaction (1)), then, more monomers were available during the growth process of the samples CM than in samples MM. The larger size of nuclei and the higher concentration of monomers during the growth process allowed samples CM to grow into larger nanoparticles. On the other hand, the influence of the IC in the size of the nanoparticle could be explained as a consequence of increasing the initial concentration of the precursor which produced smaller nuclei, however, available material to grow was also increased, allowing particles to acquire larger sizes [25].

Superparamagnetism is a magnetic behavior, in which the thermal energy exceeds the magnetic anisotropy energy and the magnetization is easily flipped. As the thermal energy depends on the temperature, superparamagnetism is observable above the blocking temperature ($T_B$), and below which, the material presents one of the classical magnetic behaviors,

ferrimagnetism in the case of magnetite [14]. The blocking temperature depends on the particle size as well as on the size distribution, the effective anisotropy constant and the experimental measuring time. Since the magnetic anisotropy energy is directly proportional to the volume of the nanoparticle, $T_B$ decreases with the depletion of nanoparticle size.

The magnetic characteristics of samples were evaluated by magnetization curves (figure 4). Results showed that all the samples exhibited superparamagnetic behavior at 300 K, since no coercivity and no hysteresis loops were observed in the curves [14].

The $M_s$ values of the nanoparticles at 300 K (table 1) were smaller than the corresponding bulk phase (90 emu g$^{-1}$); this behavior is attributed to the surface effects, as was discussed previously, the nanoparticle surface presents structural disorder, also proposed the presence of a magnetically dead layer on the particle surface and the existence of canted spins. Generally, in nanoparticles obtained at the same conditions, the surface effects become more pronounced with decreasing size of nanoparticles due to the presence of the considerably high fraction of the atoms in the surface, which explain the falling in $M_s$ with the dropping size of nanoparticles. Moreover, it is important to consider the adsorption of water and TEG molecules on the surface of the nanoparticles, this non-magnetic mass reduces the magnetization [14, 21, 30, 32].

Magnetization curves were also evaluated at 85 K. As it was expected the $M_s$ was higher at 85 K than at 300 K, this is due to the increase of thermal fluctuations of the magnetic moments of nanoparticles at higher temperatures [35, 39]. The nanoparticles also presented coercivity ($H_c$) at 85 K, indicating a ferrimagnetic regimen [30]. It is well known that at temperatures below the blocking temperature ($T < T_B$), $H_c$ increases with the decreasing of the temperature [40]. Since the values of $H_c$ of MM samples are near to zero, the $T_B$ of these samples is slightly greater than 85 K. Since the values of $H_c$ of samples CM are greater than the corresponding ones to samples MM, the $T_B$ of samples CM should be higher than those of samples MM. This is also valid if we consider that CM nanoparticles are bigger than MM nanoparticles, and greater $T_B$ is expected for the larger nanoparticles, as discussed earlier.

The figure 5(a) shows the relation between $M_s$ and nanoparticle size ($D_{TEM}$). Although the sizes of samples CM1 and CM2 nanoparticles are larger than those of samples MM2 and MM3, they display similar $M_s$. This result indicates that the surface effects are more intense in samples CM than in their counterparts MM, decreasing sharply the magnetization in the samples CM.

Assuming that the thickness ($t$) of the magnetically dead layer is near to a constant for each group of samples and $M_s{}^{bulk}$ is equal to 90 emu g$^{-1}$, $t$ was calculated by the following relation [39, 41]

$$M_s = M_s^{Bulk}\left(1 - \frac{6t}{D_{TEM}}\right). \tag{5}$$

Adv. Nat. Sci.: Nanosci. Nanotechnol. **7** (2016) 015014
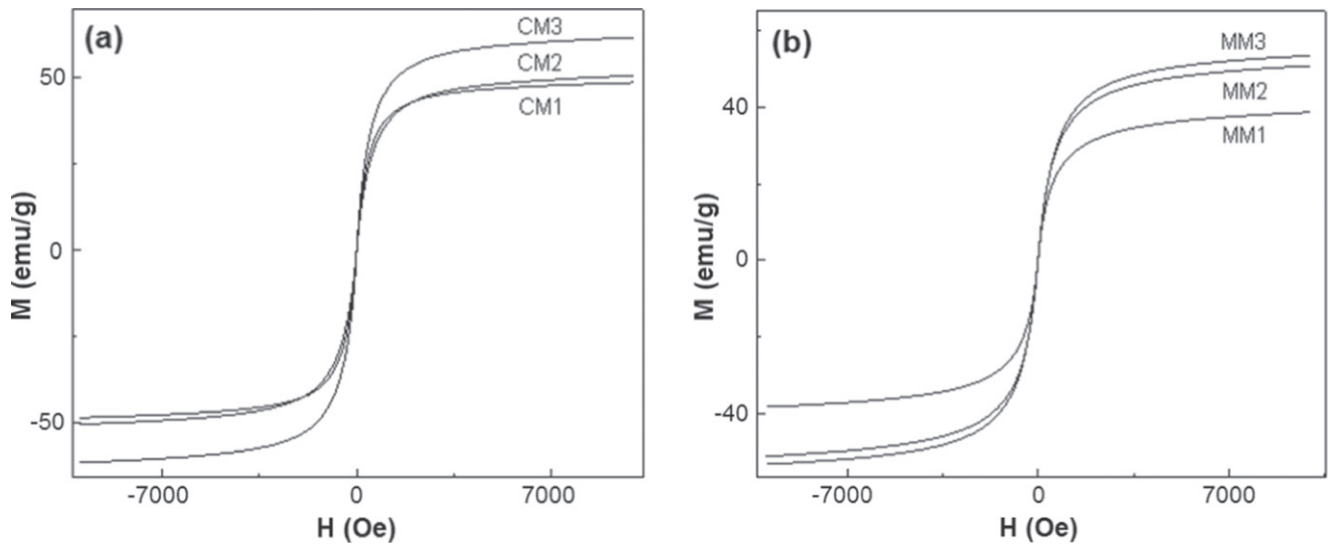
J Vega-Chacón *et al*



**Figure 4.** Magnetization curves at 300 K for magnetite samples of series (a) CM and (b) MM.
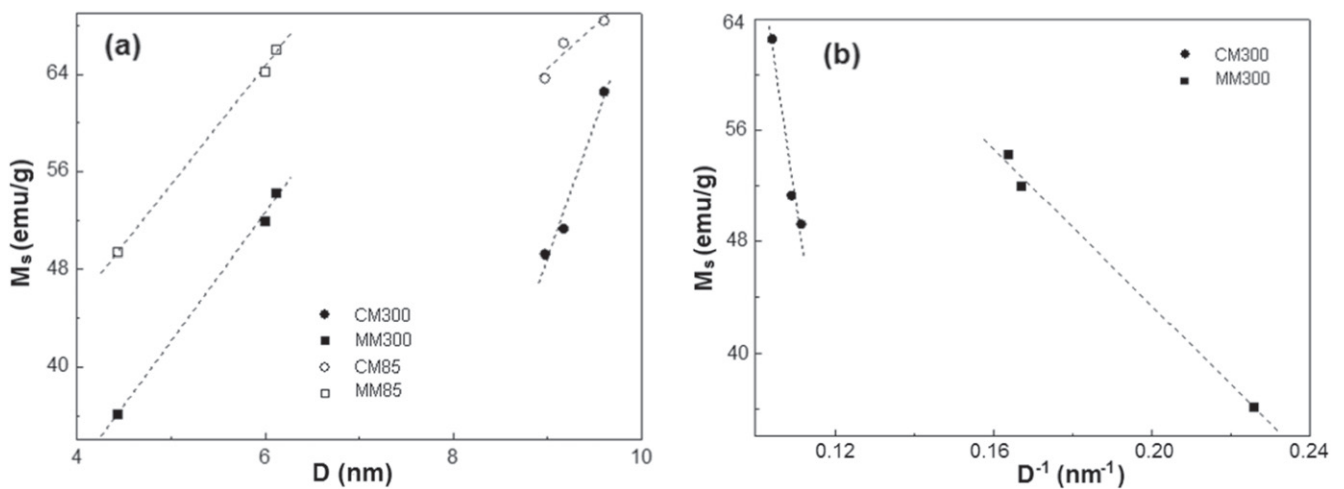


**Figure 5.** Saturation magnetization (a) $M_s$ at 300 K and 85 K as a function of nanoparticle size $D_{TEM}$ and (b) $M_s$ at 300 K as a function of the inverse of nanoparticle size $D_{TEM}^{-1}$.

As is shown in the figure 5(b), $M_s^{300K}$ as a function of $1/D_{TEM}$ can be fitted very well as a linear relationship. For nanoparticles MM, this plot matched very well with equation (5), the calculated value of $t$ was 0.5 nm, suggesting that the formation of magnetically dead layer could preferentially lead to the depletion of $M_s$. On the contrary, for nanoparticles CM, the corresponding fit differs from the equation (5), obtaining a $M_s^{bulk}$ value of 258 emu g$^{-1}$. Assuming this value as correct, the value of $t$ was 1.2 nm, and using the correct value of $M_s^{bulk}$, the value of $t$ was 3.5 nm. Both values of $t$ showed that the thickness of magnetically dead layer of samples CM is greater than the corresponding to the samples MM, so this could explain the similar $M_s$ values of CM2 and MM2 (figure 5(a)), although the differences in their average particle size. However, since the plot of samples CM disagreed with equation (5), other effects not taken into account in the equation must be considered to explain the decrease in the magnetization of samples CM.

## 4. Conclusion

Monodisperse and superparamagnetic magnetite nanoparticles were synthesized by the polyol method in hydrophilic solvent from $Fe(NO_3)_3.9H_2O$ and $Fe(acac)_3$ as precursors at different initial concentrations. The nature and the concentration of the precursor salts influence the mechanism of formation of the nanoparticles, and this also influence on the size, shape and saturation magnetization of the nanoparticles. The average particle size and the saturation magnetization of the nanoparticles increased when the initial $Fe^{3+}$ concentration was increasing. For a given $Fe^{3+}$ initial concentration, samples synthesized from $Fe(acac)_3$ produced larger nanoparticles than samples prepared from $Fe(NO_3)_3.9H_2O$. The conventional polyol method of preparation of magnetite nanoparticles uses $Fe(acac)_3$ as precursor salt, this work showed the possibility of preparing water dispersible magnetite nanoparticles starting from

Adv. Nat. Sci.: Nanosci. Nanotechnol. **7** (2016) 015014

J Vega-Chacón *et al*

Fe(NO$_3$)$_3$.9H$_2$O, a cheaper and less toxic precursor salt than its organic counterparts.

## Acknowledgments

## References

[1] Brigger I, Dubernet C and Couvreur P 2012 *Adv. Drug Deliv. Rev.* **64** 24

[2] Chomoucka J, Drbohlavova J, Huska D, Adam V, Kizek R and Hubalek J 2010 *Pharmacol. Res.* **62** 144

[3] Fan T, Li M, Wu X, Li M and Wu Y 2011 *Colloids Surf. B Biointerfaces* **88** 593

[4] Felton C, Karmakar A, Gartia Y, Ramidi P, Biris A S and Ghosh A 2014 *Drug Metab. Rev.* **46** 142

[5] Kakar S, Batra D, Singh R and Nautiyal U 2013 *J. Acute Dis.* **2** 1

[6] Reddy L H, Arias J L, Nicolas J and Couvreur P 2012 *Chem. Rev.* **112** 5818

[7] Tu Z, Zhang B, Yang G, Wang M, Zhao F, Sheng D and Wang J 2013 *Colloids Surf. A Physicochem. Eng. Asp.* **436** 854

[8] Zhang L, Dong W F and Sun H B 2013 *Nanoscale* **5** 7664

[9] Anbarasu M, Anandan M, Chinnasamy E, Gopinath V and Balamurugan K 2015 *Spectrochim. Acta. A. Mol. Biomol. Spectrosc.* **135** 536

[10] Wang Y, Nkurikiyimfura I and Pan Z 2014 *Chem. Eng. Commun.* **202** 616

[11] Keerthana D S, Namratha K, Byrappa K and Yathirajan H S 2015 *J. Magn. Magn. Mater.* **378** 551

[12] Shen K, Wang J, Li Y, Wang Y and Li Y 2013 *Mater. Res. Bull.* **48** 4655

[13] Wang J, Zhang B, Wang L, Wang M and Gao F 2015 *Mater. Sci. Eng. C Mater. Biol. Appl.* **48** 416

[14] Lu A H, Salabas E L and Schüth F 2007 *Angew. Chem. Int. Ed. Engl.* **46** 1222

[15] Rockenberger J, Scher E C and Alivisatos A P 1999 *J. Am. Chem. Soc.* **121** 11595

[16] Sun S and Zeng H 2002 *J. Am. Chem. Soc.* **124** 8204

[17] Sultana S, Khan M R, Kumar M, Kumar S and Ali M 2013 *J. Drug Target.* **21** 107

[18] Feldmann C 2003 *Adv. Funct. Mater.* **13** 101

[19] Fievet F, Lagier J P, Blin B, Beaudoin B and Figlarz M 1989 *Solid State Ion.* **33** 198

[20] Cai W and Wan J 2007 *J. Colloid Interface Sci.* **305** 366

[21] Grabs I M, Bradtmöller C, Menzel D and Garnweitner G 2012 *Cryst. Growth Des.* **12** 1469

[22] Jansch M, Stumpf P, Graf C, Rühl E and Müller R H 2012 *Int. J. Pharm.* **428** 125

[23] Maity D, Kale S N, Kaul-Ghanekar R, Xue J M and Ding J 2009 *J. Magn. Magn. Mater.* **321** 3093

[24] Miguel-Sancho N, Bomatí-Miguel O, Colom G, Salvador J P, Marco M P and Santamaría J 2011 *Chem. Mater.* **23** 2795

[25] Miguel-Sancho N, Bomati-miguel O, Roca A G, Martinez G, Arruebo M and Santamaria J 2012 *Ind. Eng. Chem. Res.* **51** 8348

[26] Günay M, Baykal A and Sözeri H 2012 *J. Supercond. Nov. Magn.* **25** 2415

[27] Jiang P, Yang X, Xin Y, Qi Y, Ma X, Li Q and Zhang Z 2012 *J. Mater. Sci.* **48** 2365

[28] Arndt D, Zielasek V, Dreher W and Bäumer M 2014 *J. Colloid Interface Sci.* **417** 188

[29] Vega J, Picasso G, Avilés L and López A 2013 *Rev. Soc. Quím. Peru* **79** 331

[30] Roca A G, Morales M P, O'Grady K and Serna C J 2006 *Nanotechnology* **17** 2783

[31] Vandenberghe R E, Nedkov I, Merodiiska T and Slavov L 2006 *Hyperfine Interact.* **165** 267

[32] Gupta A K and Gupta M 2005 *Biomaterials* **26** 3995

[33] Mandel K, Hutter F, Gellermann C and Sextl G 2011 *Colloid. Surf. A Physicochem. Eng. Asp.* **390** 173

[34] Jia X, Chen D, Jiao X and Zhai S 2009 *Chem. Commun. (Camb)* **8** 968

[35] Yang T, Shen C, Li Z, Zhang H, Xiao C, Chen S, Xu Z, Shi D, Li J and Gao H 2005 *J. Phys. Chem. B* **109** 23233

[36] Kwon S G and Hyeon T 2011 *Small* **7** 2685

[37] Park J, Joo J, Kwon S G, Jang Y and Hyeon T 2007 *Angew. Chem. Int. Ed. Engl.* **46** 4630

[38] Wan J, Cai W, Meng X and Liu E 2007 *Chem. Commun. (Camb)* **47** 5004

[39] Caruntu D, Caruntu G and O'Connor C J 2007 *J. Phys. D Appl. Phys.* **40** 5801

[40] Lin C R, Chiang R K, Wang J S and Sung T W 2006 *J. Appl. Phys.* **99** 08N710

[41] Chen J P and Sorensen C M 1996 *Phys. Rev. B* **54** 9288